CHAPTER-III

DYNAMICAL CONDUCTIVITY OF SUPERLATTICES WITH ONE CHARGE CARRIER LAYER PER UNIT CELL

Calculation of longitudinal and transverse macroscopic as well as microscopic dynamical conductivity for modulation doped type-I superlattice is reported in this chapter. Our computed long wavelength macroscopic conductivity significantly differ from Drude conductivity in low frequency regime (microwave and infra-red radiations). Macroscopic conductivity shows oscillatory behaviour along the direction of growth of superlattice. Propagation of transverse electromagnetic waves in a superlattice has been studied for all possible values of frequency and wave vector. It is found that microscopic transverse conductivity exhibits poles along both real and imaginary axis of frequency Depending on the values of wave vector components, along and perpendicular to direction of superlattice, both the poles can lie on real axis or on imaginary axis of frequency. We also find that there can be more than one penetration depths for a superlattice and one of them decreases with frequency for frequencies below microwave regime.

3.1 Introduction

Ever since their discovery, CSSL1 have been the subject of immense research interest. Extensive theoretical as well as experimental investigations have been performed on collective excitations [1-8], light scattering and Coulomb scattering [9-12], optical properties [13], transport properties [14-16] and the electrodynamical properties [5,15-19] of CSSL1. The electrodynamical studies are of great interest from the point of view of device applications and from the standpoint of fundamental physics exhibited by SL .Several interesting dynamical and static processes are induced in a SL on application of an electromagnetic field. For example, application of a electric field along the direction of growth of SL leads to unconventional transport phenomenon which attracted a great deal of recent research interests. There have been many experimental and theoretical studies focusing around the negative differential velocity, negative effective mass and negative differential conductance in the study of linear as well as non-linear vertical transport (Esaki

and Tsu conduction) in a CSSL1 [20-22]. It was suggested that the observation of negative differential conductivity along the direction of growth of SL might lead to high frequency devices.

Linear transport in SL has attracted comparatively less attention because of the belief that it could be understood in terms of Drude type theories. There have been some theoretical studies on linear conductivity along the plane perpendicular to the direction of growth of SL [16,23,24]. However, most of these calculations of conductivity of SL have been performed for special cases of wave vector and frequency and none of these is valid for all values of wave vector and frequency. Also, the important effects such as those arising from intersubband transitions (finite width of electron layer), interlayer interactions, wave vector dependence in low and high frequency regime and the change in dimension from 3D to 2D are not properly incorporated in these studies. Several interesting and new features of dynamical linear conductivity along the direction of growth and in the plane perpendicular to the direction of growth of a SL emerge out in different regimes of wave vector and frequency. These features cannot be explained by existing calculations. This has been main motivation to take up the theoretical study presented in this chapter

Application of electromagnetic field to a system excites collective excitations. Recently it has been shown that screened longitudinal polarizability function of 2DEG when calculated RPA shows poles on imaginary axis of frequency, ω [25]. It is said that poles on imaginary axis of ω represent a 'collective state', which has been called as ghost plasmons. Recent experimental data on 2D electron system suggests that an electron system shows negative compressibility This is a direct evidence of existence of ghost plasmons because negative compressibility means the negative dielectric function [26]. Pines and Nozieres [27] had shown that poles in screened polarizability at imaginary axis of ω implies that longitudinal dielectric function is not analytic in upper half plane of complex ω and it leads to a negative value of static dielectric function which means overscreening

The present theoretical approach employs the Maxwell's equations and continuity equation to develop real space formalism of dynamical conductivity in terms of density response function, current response function and the dielectric response function. Presently developed real space formalism of conductivity takes into account the possibility of conduction along the direction of growth and along the plane perpendicular to direction of growth of a CSSL1. It properly incorporates all kinds of dynamical and static processes along

with screening effects arising from many body electron-electron interactions. We calculated both longitudinal and transverse conductivities in the absence of magnetic field at zero temperature and we have studied them for all possible values (real as well as imaginary) of wave vector and frequency for CSSL1. In comparison with existing theoretical work on linear conductivity, the present theoretical study being more rigorous is valid for 2D and 3D limits. The calculation is applied to $Al_xGa_{1-x}As/GaAs$ CSSL1. This chapter is organized in four sections. Formalism and calculation of longitudinal and transverse conductivities are given in section 3.2. Macroscopic and microscopic dynamical conductivity have been discussed under various limits in section 3.3 and 3.4. respectively. This chapter is concluded in sec.3.5.

3.2 Formalism and Calculations of Conductivity

The longitudinal/transverse macroscopic conductivity, $\sigma^{L/T}(\mathbf{r},\mathbf{r}',\omega)$ and microscopic conductivity $\tilde{\sigma}^{L/T}(\mathbf{r},\mathbf{r}',\omega)$ are reported in chapter-II. Evaluation of $\sigma(\mathbf{r},\mathbf{r}',\omega)$ and $\tilde{\sigma}(\mathbf{r},\mathbf{r}',\omega)$ for both longitudinal as well as transverse field basically depends on calculation of density response function. Equations (2.5a), (2.18) and (2.29) describe generalized longitudinal and transverse dynamical conductivities in the form of self-consistent equations. These equations are in real space and they have wide applicability

Neglecting the difference in dielectric constants of layers in a unit cell, of length d in direction of growth, a CSSL1 can be modelled to be a periodic sequence of layers of charge carriers embedded into a homogeneous dielectric medium of dielectric constant, ε_0. It is further assumed that, (i) electrons are confined to layers and there is no overlap between the wave functions of adjoining layers, (ii) an electron executes free particle motion with effective mass, m^* in x-y plane. We first Fourier transform Eqs.(2.5a), (2.18) and (2.29) in x-y plane and we obtain

$$\sigma^{L/T}(\mathbf{q},z,z',\omega) = (\gamma - i\omega/4\pi)\int V(\mathbf{q},z,z'')\alpha^{L/T}(\mathbf{q},z'',z',\omega)dz'', \qquad (3.1)$$

$$\tilde{\sigma}^{L}(\mathbf{q},z,z',\omega)=\sigma^{L}(\mathbf{q},z,z',\omega)-\iint\tilde{\sigma}^{L}(\mathbf{q},z,z_1,\omega)V(\mathbf{q},z_1,z_2)\alpha^{L}(\mathbf{q},z_2,z',\omega)\, dz_1dz_2, \qquad (3.2)$$

$$\tilde{\sigma}^{T}(\mathbf{q},z,z',\omega) = \sigma^{T}(\mathbf{q},z,z',\omega) + (i\omega/c^2)\iint\tilde{\sigma}^{L}(\mathbf{q},z,z_1,\omega)\, G(\mathbf{q},z_1,z_2,\omega)\, \sigma^{T}(\mathbf{q},z_2,z',\omega)\, dz_1\, dz_2 \qquad (3.3)$$

with

$$V(\mathbf{q},z_1,z_2) = (2\pi e^2/\mathbf{q}) \exp(-\mathbf{q}| z_1-z_2|) \tag{3.4a}$$

and

$$G(\mathbf{q},z_1,z_2,\omega) = (2\pi/\mathbf{p}) \exp(-\mathbf{p}| z_1-z_2|), \tag{3.4b}$$

where

$$\mathbf{p}=[\mathbf{q}^2 -(\omega^2/c^2)]^{1/2}. \tag{3.4c}$$

We further consider the case of superlattice where electrons and holes are mainly confined to their respective layers (non-tunnelling case). Confinement of motion gives rise to discrete energy levels along z-axis. For an electron in nth level of lth layer, envelope function is given by

$$\phi_{nl}(\mathbf{z}) = (2/L)^{1/2} \sin \{(n+1)\pi[(z-ld)/L+1/2]\}, \tag{3.5}$$

where L is the width of electron layer. On defining z-ld=t with $-L/2 \le t \le L/2$, Eqs.(3.1) to (3.4) can be transformed to

$$\sigma^{L/T}(\mathbf{q},l,l',t,t',\omega)=(\gamma i\omega/4\pi)\sum_{l''}\int V(\mathbf{q},l,l'',t,t'')\alpha^{L/T}(\mathbf{q},l'',l',t'',t',\omega)dt'', \tag{3.6}$$

$$\tilde{\sigma}^{L}(\mathbf{q},l,l't,t',\omega)=\sigma^{L}(\mathbf{q},l,l',t,t',\omega)+\sum_{l_1}\iint\tilde{\sigma}^{L}(\mathbf{q},l,l_1,t,t_1,\omega)V(\mathbf{q},l_1,t_1,l',t_2)$$

$$\alpha^{L}(\mathbf{q},t_2,t',\omega)\, dt_1\, dt_2, \tag{3.7a}$$

$$\tilde{\sigma}^{T}(\mathbf{q},l,l't,t',\omega)=\sigma^{T}(\mathbf{q},l,l',t,t',\omega)+(i\omega/c^2)\sum_{l_1,l_2}\iint dt_1\, dt_2\tilde{\sigma}^{T}(\mathbf{q},l,l_1,t,t_1,\omega)$$

$$G(\mathbf{q},l_1,t_1,l_2,t_2,\omega)\, \sigma^{T}(\mathbf{q},l_2,l',t_2,t',\omega) \tag{3.7b}$$

with

$$V(\mathbf{q},l,l',t,t')=(2\pi e^2/\mathbf{q}) \exp[-\mathbf{q}| (l-l')d+(t-t')|] \tag{3.8a}$$

and

$$G(\mathbf{q},l,l',t,t',\omega)=(2\pi/\mathbf{p}) \exp[-\mathbf{p}| (l-l')d+(t-t')|]. \tag{3.8b}$$

With the use of discrete Fourier transform

$$f(\mathbf{q},q_z,\omega) = \sum_{l-l'} f(\mathbf{q},l,l',\omega)\exp[-iq_z(l-l')d] \qquad (3.9)$$

we get

$$\sigma^{L/T}(\mathbf{q},q_z,\omega) = [(\gamma-i\omega)e^2/2\mathbf{q}]e^2\,\alpha_e^{L/T}(\mathbf{q},\omega)U(\mathbf{q},q_z) - (i\omega/4\pi)\,(\varepsilon_0-1). \qquad (3.10)$$

Equation (3.10) represents macroscopic conductivity due to electrons and ions. Similarly, Fourier transform of Eqs.(3.7a) and (3.7b) give

$$\tilde{\sigma}^{L}(\mathbf{q},q_z,\omega) = \sigma^{L}(\mathbf{q},q_z,\omega) / \varepsilon^{L}(\mathbf{q},q_z,\omega) \qquad (3.11)$$

and

$$\tilde{\sigma}^{T}(\mathbf{q},q_z,\omega) = \sigma^{T}(\mathbf{q},q_z,\omega) / F(\mathbf{q},q_z,\omega), \qquad (3.12)$$

with

$$F(\mathbf{q},q_z,\omega) = [1-((\omega+i\gamma)^2d/2\mathbf{p}c^2)\,U(\mathbf{p},q_z)\,[\varepsilon^{T}(\mathbf{q},q_z,\omega)-1] \qquad (3.13)$$

and

$$\varepsilon^{L/T}(\mathbf{q},q_z,\omega)=\varepsilon_0+(2\pi e^2/\mathbf{q})\,U(\mathbf{q},q_z)\,\alpha_e^{L/T}(\mathbf{q},\omega). \qquad (3.14)$$

The structure factor $U(\mathbf{q}.q_Z)$ is given by

$$U(\mathbf{q},q_z) = H(\mathbf{q})-C(\mathbf{q})\{1-[\sinh(\mathbf{q}d)/(\cosh(\mathbf{q}d)-\cos(q_zd))]\}. \qquad (3.15)$$

$U(\mathbf{p},q_Z)$ is obtained from (3.15) on replacing $\mathbf{q}$ by $\mathbf{p}$. The $H(\mathbf{q})$ and $C(\mathbf{q})$ are the expectation values of $\exp(-\mathbf{q}|\,t-t'|\,)$ and $\exp[-\mathbf{q}(t-t')]$, respectively The $H(\mathbf{q})$ is defined as

$$H(\mathbf{q}) = \int_{-L/2}^{L/2} dt \int_{-L/2}^{L/2} dt'\, \exp[-\mathbf{q}|\,t-t'|\,]\,|\,\phi(t)|^2\,|\,\phi(t')|^2 \qquad (3.16)$$

and $C(\mathbf{q})$ is obtained from Eq.(3.16) on replacing $\mathbf{q}|\,t-t'|$ by $\mathbf{q}(t-t')$. Equation (3.10) to (3 15) are applicable for both intrasubband as well as intersubband transition. In following we consider only intrasubband transition case (n=0). Evaluation of (3.16) with the use of Eq.(3 5), for intrasubband transition, gives

$$H(\mathbf{q}) = [u/x+2/u] - 32\,(\pi^2/xu)^2\,[1-\exp(-u)]$$

and

$$C(\mathbf{q}) = g(\mathbf{q})\,g(-\mathbf{q}) \qquad (3.18)$$

with

$$g(\mathbf{q}) = (4\pi^2/xu)\,[1-\exp(-u)], \qquad (3.19)$$

where $u = qL$ and $x = u^2 + 4\pi^2$. The $\alpha_e^L(\mathbf{q},\omega)$ and $\alpha_e^T(\mathbf{q},\omega)$ are longitudinal and transverse 2D polarization functions, respectively. We consider the case of a modulation doped CSSL1, where RPA can be used to calculate $\alpha_e^{L/T}(\mathbf{q},\omega)$. The RPA expression of $\alpha_e^L(\mathbf{q},\omega)$ is given by [28]

$$\alpha_e^L(\mathbf{q},\omega)=(m^* k_F/\pi\hbar^2\mathbf{q})\{[((\omega+i\gamma)/\mathbf{q}v_F-\mathbf{q}/2k_F)^2-1]^{1/2}-[(\omega+i\gamma)/\mathbf{q}v_F-\mathbf{q}/2k_F] - [((\omega+i\gamma)/\mathbf{q}v_I+\mathbf{q}/2k_F)^2-1]^{1/2}+[(\omega+i\gamma)/\mathbf{q}v_F+\mathbf{q}/2k_F]\}, \qquad (3.20)$$

where v_F and k_F are 2D Fermi velocity and Fermi wave vector, respectively. Within RPA, $\alpha_e^T(\mathbf{q},\omega)$ can be given by [16]

$$\alpha_e^T(\mathbf{q},\omega) = [\mathbf{q}^2/(\omega+i\gamma)^2]\,[\chi(\mathbf{q},\omega) + n_s/m^*], \qquad (3.21)$$

where n_S is the number of electrons per unit area and $\chi(\mathbf{q},\omega)$ is 2D free electron current-current response function We evaluated $\chi(\mathbf{q},\omega)$ to obtain

$$\alpha_e^T(\mathbf{q},\omega)=-(m^*/\pi\hbar^2)\{1+(\mathbf{q}v_F/3(\omega+i\gamma))\{[(k_Fv_F/(\omega+i\gamma))((\omega+i\gamma)^2/(\mathbf{q}v_F)^2-1)-1] [((\omega+i\gamma)/\mathbf{q}v_F-\mathbf{q}/2k_F)^2-1]^{1/2}-[(k_Fv_F/(\omega+i\gamma))((\omega+i\gamma)^2/(\mathbf{q}v_F)^2-1)+1] [((\omega+i\gamma)/\mathbf{q}v_I+\mathbf{q}/2k_F)^2-]^{1/2}\}\}, \qquad (3.22)$$

Equations (3.20) and (3.22) are valid for all values of ω and $\mathbf{q}\leq 2k_F$ Equations (3.10) to (3.15) describe dynamical linear conductivities for all value of $\mathbf{q}$, q_Z, ω, γ and n_S. However, in following we analyze our results for different special cases of low frequency regime in non-retardation limit ($\omega<<qc$). Zeroes of $\varepsilon^L(\mathbf{q},q_Z,\omega)$ give frequencies of longitudinal collective excitations whereas zeroes of $F(\mathbf{q},q_Z,\omega)$ yield frequencies of transverse collective

excitations in a CSSL1. Several types of TE and TM modes have been calculated for CSSL1 [15-18]. However, the discussion of these modes was mostly confined to long wavelength limit. For the case of L much smaller than d, the CSSL1 reduces to LEG. The LEG results can be obtained from Eqs.(3.10) to (3.15) and (3.20) to (3.22) on taking $L\rightarrow 0$ limit of $H(\mathbf{q})$ and $C(\mathbf{q})$. Our calculated $\sigma^{L/T}(\mathbf{q},q_z,\omega)$ and $\tilde{\sigma}^{L/T}(\mathbf{q},q_z,\omega)$ can be decomposed into components along x-y plane and along z-axis (direction of CSSL1). However, in our formalism electron motion is assumed to be confined to x-y plane and no electron momentum transfer can take place along z-axis for $\mathbf{q}=0$, hence $\sigma^{L/T}(q_z,\omega)\equiv\tilde{\sigma}^{L/T}(q_z,\omega)=0$.

3.3 Macroscopic conductivity

From viewpoint of utility of our calculation in explanation of experimental results, we consider the case $\mathbf{q}<<k_F$ and $\omega<<\mathbf{q}c$. On expanding Eqs.(3.20) and (3.22) for $\mathbf{q}<<k_F$, we find that $\alpha_e^L(\mathbf{q},\omega)$ and $\alpha_e^T(\mathbf{q},\omega)$ can be related in following manner [16];

$$\alpha_e^T(\mathbf{q},\omega) = \alpha_e^L(\mathbf{q},\omega) / [1-(\pi h^2/m^*)\,\alpha_e^L(\mathbf{q},\omega)] \qquad (3.23)$$

which yields correct values of $\alpha_e^T(\mathbf{q},\omega)$ for both the limits of $(\omega+i\gamma)>>\mathbf{q}k_F$ and $\omega\rightarrow 0$. Equation (3.10), with the use of Eqs.(3.20) and (3.22), gives

$$\sigma^L(\mathbf{q},q_z,\omega)=[(\gamma-i\omega)/2\pi\mathbf{q}a^*]\{1+[(\eta^2-1-\eta\bar{\mathbf{q}})^{1/2}-(\eta^2-1+\eta\bar{\mathbf{q}})^{1/2}]/\bar{\mathbf{q}}\}U(\mathbf{q},q_z) \qquad (3.24a)$$

and

$$\sigma^T(\mathbf{q},q_z,\omega) = -[(\gamma-i\omega)/2\pi\mathbf{q}a^*]\{1+1/3\eta)\,[(\eta^2-1)/\eta\bar{\mathbf{q}}-1)(\eta^2-1-\eta\bar{\mathbf{q}})^{1/2}-((\eta^2-1)/\eta\bar{\mathbf{q}}+1)\,(\eta^2-1+\eta\bar{\mathbf{q}})^{1/2}]\}U(\mathbf{q},q_z), \qquad (3.24b)$$

where $\bar{\mathbf{q}}=\mathbf{q}/k_F$, $\eta=(\omega+i\gamma)/\mathbf{q}v_F$ and $a^*=\hbar^2/m^*e^2$ is effective Bohr radius. In Eqs.(3.24a) and (3.24b), we have dropped ionic contribution to conductivity. Our computed normalized $\sigma_R^L(\mathbf{q},q_z,\omega)$ and $\sigma_R^T(\mathbf{q},q_z,\omega)$, real part of $\sigma^L(\mathbf{q},q_z,\omega)$ and $\sigma^T(\mathbf{q},q_z,\omega)$ respectively, are plotted in Fig.3.1 as function of ω for two values of $\mathbf{q}d$ (0.001 and 0.1) at $q_zd=0$, $n_s=7.3\times10^{11}$ cm^{-2} and $\gamma=0.1$ meV for GaAs/Al_xGa_{1-x}As CSSL1, which is modelled in terms of following values of parameters: $m^*=0.068\ m_e$, d=500 Å, L=252 Å and $\varepsilon_0=13.1$ [12]. Computed $\sigma_R^L(\mathbf{q},q_z,\omega)$ shows a peak near $\omega=\mathbf{q}v_F$ and $\sigma_R^L(\mathbf{q},q_z,\omega)\equiv\sigma_R^T(\mathbf{q},q_z,\omega)$ at $\omega=\mathbf{q}v_F/\sqrt{2}$ for given value of $\mathbf{q}$ and q_z. For single particle excitation, $\hbar\omega=E_{\mathbf{k}+\mathbf{q}}-E_{\mathbf{k}}$, which for an electron at

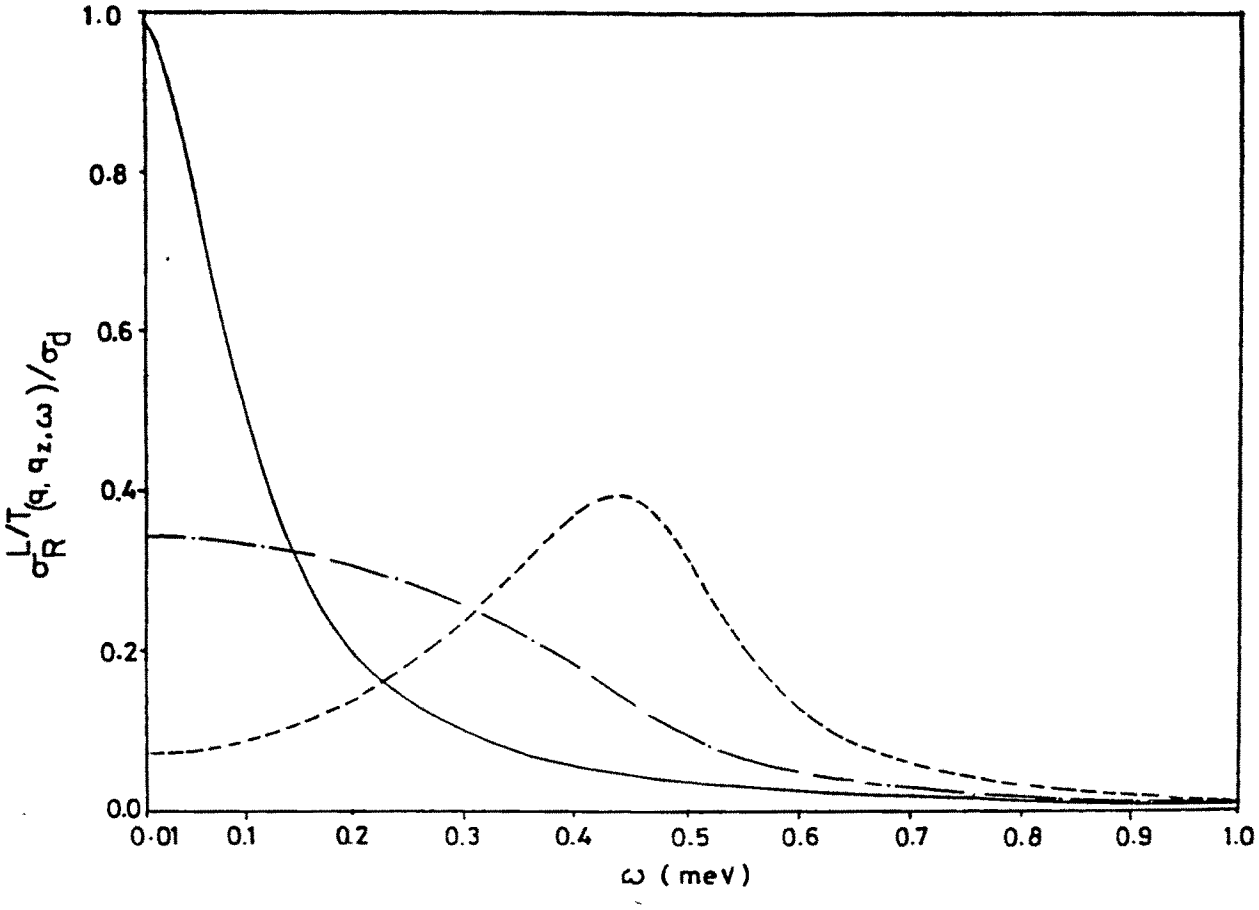

Fig. 3.1 Plot of $\sigma_R^{L/T}(\mathbf{q},q_z,\omega)/\sigma_d$ versus ω at $\cos(q_z d)=1$ For $qd=0.001$. $\sigma_R^{L}(\mathbf{q},q_z\,\omega)$ coincides with $\sigma_R^{T}(\mathbf{q},q_z,\omega)$ and each of them is shown by solid curve The dash-dash curve is $\sigma_R^{L}(\mathbf{q},q_z,\omega)$ for $qd=0.1$. whereas dash-dot curve is $\sigma_R^{T}(\mathbf{q},q_z,\omega)$ for $qd=0.1$ These curve are obtained for $n_s=7\ 3\times10^{11}$ cm^{-2} and γ = 0.1 meV with σ_d = $n_s e^2/\gamma m^* d$

Fermi surface and for the case of $q<<k_F$ yields $\omega \sim qv_F \cos\theta$, where θ is angle between **k** and **q**. For the case of forward scattering, $\theta=0$ and one obtains $\omega \sim qv_F$. We thus find that peak in $\sigma_R^L(q,q_z,\omega)$ around $\omega \sim qv_F$ corresponds to single particle excitations for forward scattering case. The averaged mean square value of ω for single particle excitations when $q<<k_F$ is given by $\omega \sim qv_F/\sqrt{2}$, where $\sigma_R^L(q,q_z,\omega)$ and $\sigma_R^T(q,q_z,\omega)$ intersect each other. It is found that position of peak in $\sigma_R^L(q,q_z,\omega)$ is independent of q_z, whereas peak height increases on changing $\cos(q_z d)$ from 1 to -1 It also enhances on increasing qd at fixed value of $q_z d$. The **q**-dependence of peak height has been found to be weaker in case of $\cos(q_z d)=1$, as compared with that for $\cos(q_z d) = -1$. In long wavelength limit ($qd<<1$ and $q_z d<<1$) Eq.(3.15) reduces to

$$U(q,q_z) \sim 2q/(q^2+q_z^2)d. \qquad (3.25)$$

We further find that for the case of $|\eta| >>1$, $qd \to 0$ and $q_z d \to 0$, $\sigma_R^L(q,q_z,\omega) \cong \sigma_R^T(q,q_z,\omega)$ and each of them is given by

$$\sigma_d(\omega) = n_s e^2/m^* d\,(\gamma - i\omega), \qquad (3.26)$$

which is well known Drude relation of conductivity, in our notations. However, $\sigma_R^L(q,q_z,\omega)$ and $\sigma_R^T(q,q_z,\omega)$ significantly differ from $\sigma_d(\omega)$ when $|\eta| \sim 1$ The condition $|\eta| \sim 1$ in the case of $qd<<1$ and $q_z d=0$ can be fulfilled at small ω-values (microwave and infrared frequency regimes) if γ and m^* are small and n_s is large In a modulation doped CSSL1, electrons reside in wells, whereas doped impurities are confined to barriers to yield smaller value of γ. A rough estimate of γ can be made by using the relation $\gamma = e/m^*\mu$ Depending on value of μ, γ can vary from 0.01 meV to 0.1 meV in modulation doped CSSL1 [29]. Recently, $\mu = 1.05 \times 10^7$ $cm^2V^{-1}s^{-1}$ at 1.5K has been obtained in modulation doped $GaAs/Al_xGa_{1-x}As$ [30] which suggests that γ can be as low as 1.6×10^{-3} meV Therefore, $|\eta| >>1$ is not fulfilled even for $q \sim 10^2$ cm^{-1} and $q_z d=0$ in microwave frequency regime This suggests that the use of Drude relation to explain dynamical conductivity in microwave and infrared frequency regimes can be highly erroneous in a modulation doped CSSL1. Also, $\sigma_R^L(q,q_z,\omega) \neq \sigma_R^T(q,q_z,\omega)$ for $|\eta|$ not much larger than unity. Computed $\sigma_R^L(q,\omega)/\sigma_d(\omega)$ and $\sigma_R^T(q,\omega)/\sigma_d(\omega)$ are plotted as a function of ω for $\omega<\omega_p$ at $q_z d=0$, $\gamma = 8.475 \times 10^{-3}$ meV, $n_S = 10^{12}$ cm^{-2} for $qd=0.001$ and $qd=0.005$ [31] in Fig.3.2. It can be noted from the figure

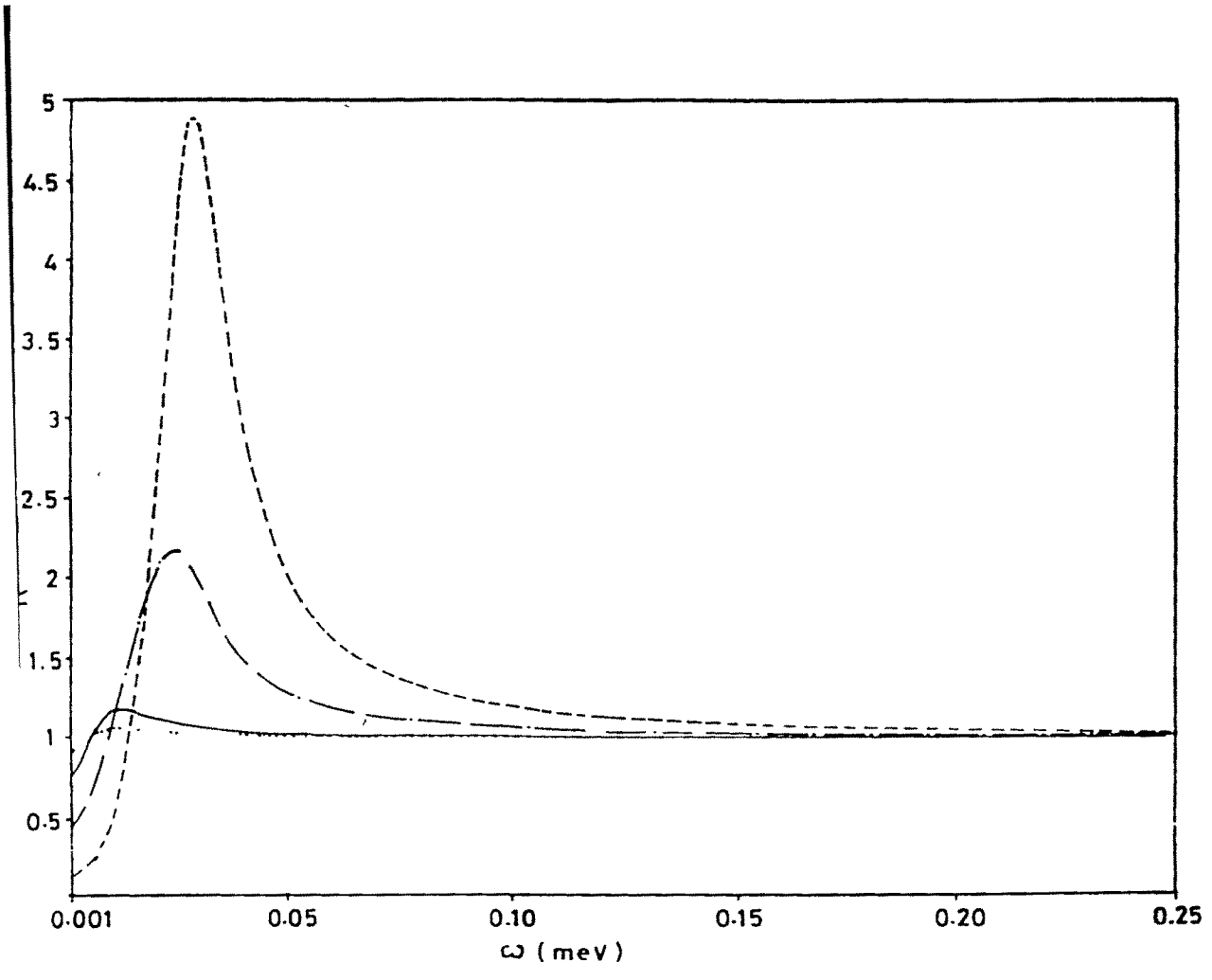

Fig. 3.2 The $\sigma_R^L(\mathbf{q},q_z,\omega)/\sigma_d(\omega)$ (solid line curve for **q**d=0.001 and dash-dash curve for **q**d=0 005) and $\sigma_R^T(\mathbf{q},q_z,\omega)/\sigma_d(\omega)$ (dot-dot curve for **q**d=0 001 and dash-dot curve for **q**d=0.005) plotted as a function of ω at $\gamma = 8.475 \times 10^{-3}$ meV, $n_s = 10^{12}$, cm^{-2} and $\cos(q_z d)=1$.

that $\sigma_R^L(\mathbf{q},\omega)/\sigma_d(\omega)$ and $\sigma_R^T(\mathbf{q},\omega)/\sigma_d(\omega)$ are significantly different from unity at both values of $\mathbf{q}d$ for ω belonging to microwave and infrared frequency regimes.

It is found that the behavior of our computed $\sigma_R^{L/T}(\mathbf{q},q_z,\omega)$ versus ω, for given $\mathbf{q}$ and q_z is identical to that versus $\mathbf{q}$, for given ω and q_z. We further find that the behavior of $\sigma_R^{L/T}(\mathbf{q},q_z,\omega=0)$ with $\mathbf{q}$ is almost identical to that with q_z for $\mathbf{q}\geq q_z$ $0\leq\cos(q_zd)\leq 1$. $\sigma_R^L(\mathbf{q})$ ($\sigma_R^L(\mathbf{q},q_z,\omega)$ when $q_z\equiv\omega\equiv 0$) shows $1/\mathbf{q}^2$-dependence, whereas real part of $\sigma_d(\omega)$ exhibit $1/\omega^2$-dependence for $\gamma^2<<\omega^2$. For the case of single particle excitations, where $\mathbf{q}$ can be replaced by $\sqrt{2}\eta$, $\sigma^L(\mathbf{q})$ goes over to $\sigma_d(\omega)$. It can therefore be concluded that each of $\sigma_R^{L/T}(\mathbf{q},\omega)$, $\sigma_R^{L/T}(q_z,\omega)$ and $\sigma_R^{L/T}(\mathbf{q},q_z)$ describes dynamical conductivity. Therefore, the conduction along the direction of growth of SL can be studied by calculating $\sigma_R^{L/T}(\mathbf{q},q_z)$ as a function of q_z. On rewriting Eqs.(3.24a) and (3.24b) for $\omega\rightarrow 0$, we obtain

$$\sigma^L(\mathbf{q},q_z)=(\gamma/2\pi\mathbf{q}a')\{1+i[(\eta_2^2+1+i\eta_2\bar{\mathbf{q}})^{1/2}-(\eta_2^2+1-i\eta_2\bar{\mathbf{q}})^{1/2}]/\bar{\mathbf{q}}\}\,U(\mathbf{q},q_z) \tag{3.27a}$$

and

$$\sigma^T(\mathbf{q},q_z)=(\gamma/2\pi\mathbf{q}a')\{1+(1/3\eta_2)[i((\eta^2+1)/\eta_2\bar{\mathbf{q}}-1)(\eta_2^2+1+i\eta_2\bar{\mathbf{q}})^{1/2}]-$$
$$[i((\eta^2+1)/\eta_2\bar{\mathbf{q}}+1)(\eta_2^2+1-i\eta_2\bar{\mathbf{q}})^{1/2}]\}U(\mathbf{q},q_z), \tag{3.27b}$$

where $\eta_2=\gamma/\mathbf{q}v_F$. Both Eqs (3.27a) and (3.27b) reduce to d.c conductivity

$$\sigma_d = n_s e^2/\gamma m^* d, \tag{3.27c}$$

for the case of $\eta_2>>1$ and $q_zd<<\mathbf{q}d<<1$. Whereas for η_2 not much larger than unity, $\sigma^L(\mathbf{q},q_z) < \sigma^T(\mathbf{q},q_z)$ at all values of $\mathbf{q}$, q_z and n_s. It is found that computed $\sigma_R^{L/T}(\mathbf{q},q_z)$ as a function of $\mathbf{q}$, at a non-zero value of q_z, first increases and then declines after passing over a maximum which occurs at $\mathbf{q}=q_z$. The magnitude of maximum depends on q_z and it has highest value ($=\sigma_d$) at $q_z=0$. for a given value of $\mathbf{q}$ $\sigma_R^{L/T}(\mathbf{q},q_z)$ versus $\mathbf{q}$ exhibits only one maximum. On the other hand $\sigma_R^{L/T}(\mathbf{q},q_z)$ as a function of q_z exhibits an oscillatory behavior which is a characteristic of a periodic structure. The maxima occur at $q_z=2m\pi/d$, whereas minima occur at $q_z=(2m+1)\pi/d$, where $m=0,1,2..$ for given value of $\mathbf{q}$. Our computed $\sigma_R^L(\mathbf{q},q_z)$ and $\sigma_R^T(\mathbf{q},q_z)$ as a function of q_zd at different values of d, n_S, L and $\mathbf{q}$. Our computed $\sigma_R^T(\mathbf{q},q_z)$ at $\gamma=0.1$ meV and $n_S=3.0\times10^{11}$ cm^{-2} [29] is plotted as a function of q_zd

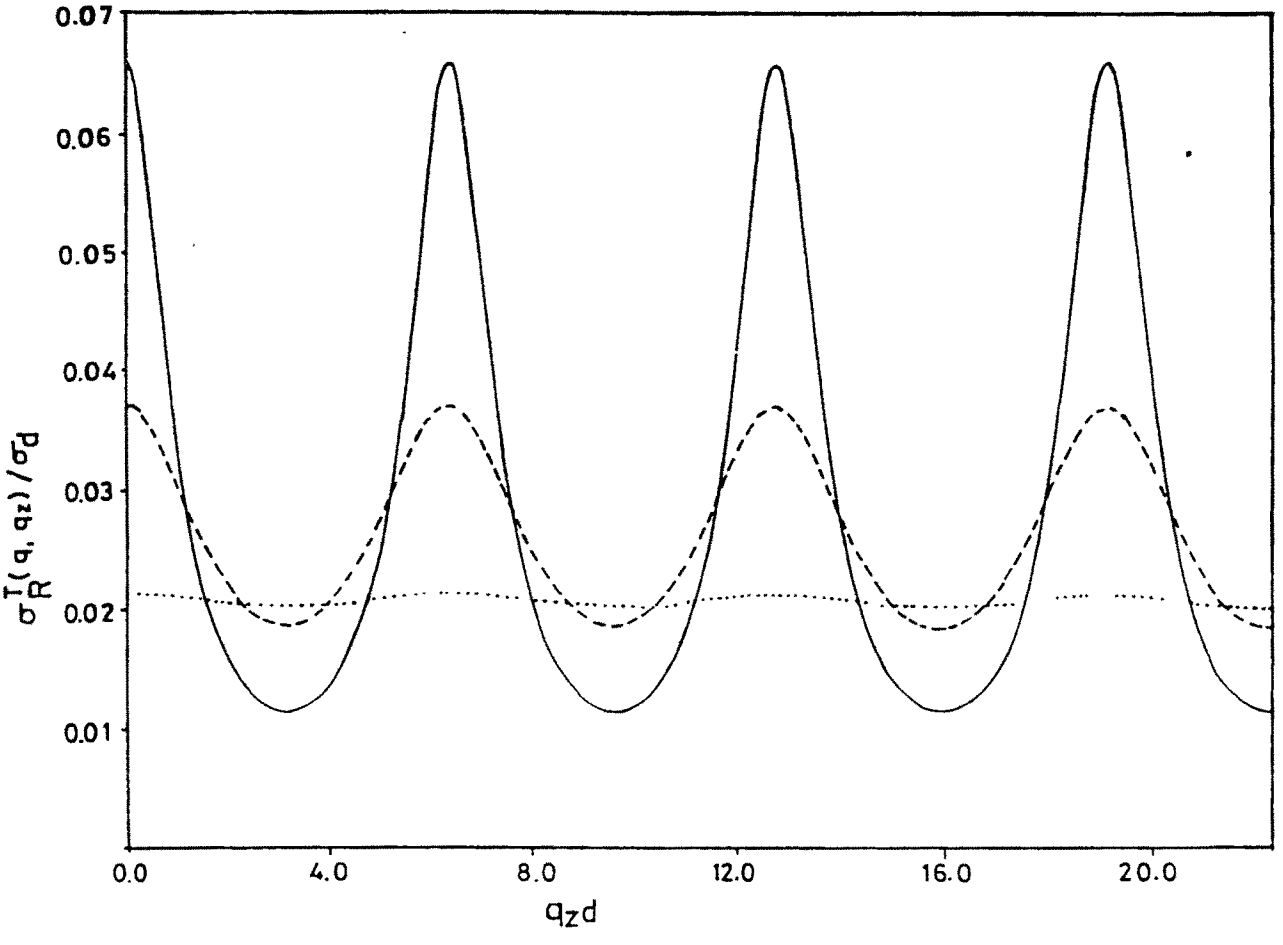

Fig. 3.3 A plot of $\sigma_R^T(\mathbf{q},q_z)/\sigma_d$ versus $q_z d$ for $\mathbf{q}d=1.0$ (solid line curve), $\mathbf{q}d=2.0$ (dash-dash curve) and $\mathbf{q}d=5.0$ (dotted curve) at $\cos(q_z d)=-1$, $n_s=3.0\times10^{11}$ cm^{-2} and $\gamma=0.1$meV

for three values of **qd** (1.0, 2.0, 5.0) in Fig.3.3. Values of rest of the parameters are taken same as used earlier. The value of wavelength, which corresponds to q_z used to obtain Fig.3.3 lie in infrared radiation regime. It can be seen from the figure that amplitude of oscillation decreases on increasing **qd** and lower peak is broader as compared to upper peak. The **qd** can be enhanced on increasing d when **q** is kept fixed. The increase in d reduces the anisotropy and it takes the SL more closer to 3D solid. The layered structure of SL works like a filter of conductivity where amplitude of oscillations can be controlled by changing d for fixed **q** and by changing **q** for fixed value of d. Similar type of oscillations have experimentally been observed in microwave conductance along the direction of growth of a tunneling GaAs/AlAs SL [20]. These oscillations have been attributed to negative differential conductivity along the direction of growth of a tunneling GaAs/AlAs SL. It is to be noted that our Eqs.(3.10)-(3.15) are applicable to a non-tunneling SL. However, our real space formalism are applicable to both non-tunneling as well as tunneling SL. Inclusion of tunneling along z-axis is expected to change absolute magnitude of conductivity and amplitude of oscillations along z-axis. However, the oscillatory behavior of conductivity, which characterizes periodic structure of SL along z-axis, will still be there. The $\sigma_R^L(\mathbf{q},q_z)$ as a function of $q_z d$ exhibits oscillatory behavior which is similar to that of $\sigma_R^T(\mathbf{q},q_z)$ as a function of $q_z d$. However, $\sigma_R^T(\mathbf{q},q_z) >> \sigma_R^L(\mathbf{q},q_z)$ for $1.0 \leq qd \leq 5.0$ Amplitude of oscillations has also been found to decrease on increasing n_s.

3.4 Microscopic conductivity

The microscopic conductivity is given by Eqs.(3.11) and (3.12), where the effects of screening are incorporated in $\varepsilon^L(\mathbf{q},q_z,\omega)$ and $F(\mathbf{q},q_z,\omega)$. Propagation of various types of electromagnetic modes with and without including retardation effects in LEG and CSSL1 have been discussed by several authors for different wave vector regimes [6,8,15-18]. We here discuss only those electromagnetic modes which are given by $\varepsilon^L(\mathbf{q},q_z,\omega)$ and $F(\mathbf{q},q_z,\omega)$ For the case of $q << k_F$, $\varepsilon^L(\mathbf{q},q_z,\omega)$ and $F(\mathbf{q},q_z,\omega)$ can be written as

$$\varepsilon^L(\mathbf{q},q_z,\omega) = \varepsilon_0 + (2/qa)\{1 + [(\eta^2 - 1 - \eta\bar{q})^{1/2} - (\eta^2 - 1 + \eta\bar{q})^{1/2}]/\bar{q}\}U(\mathbf{q},q_z) \tag{3.28}$$

and

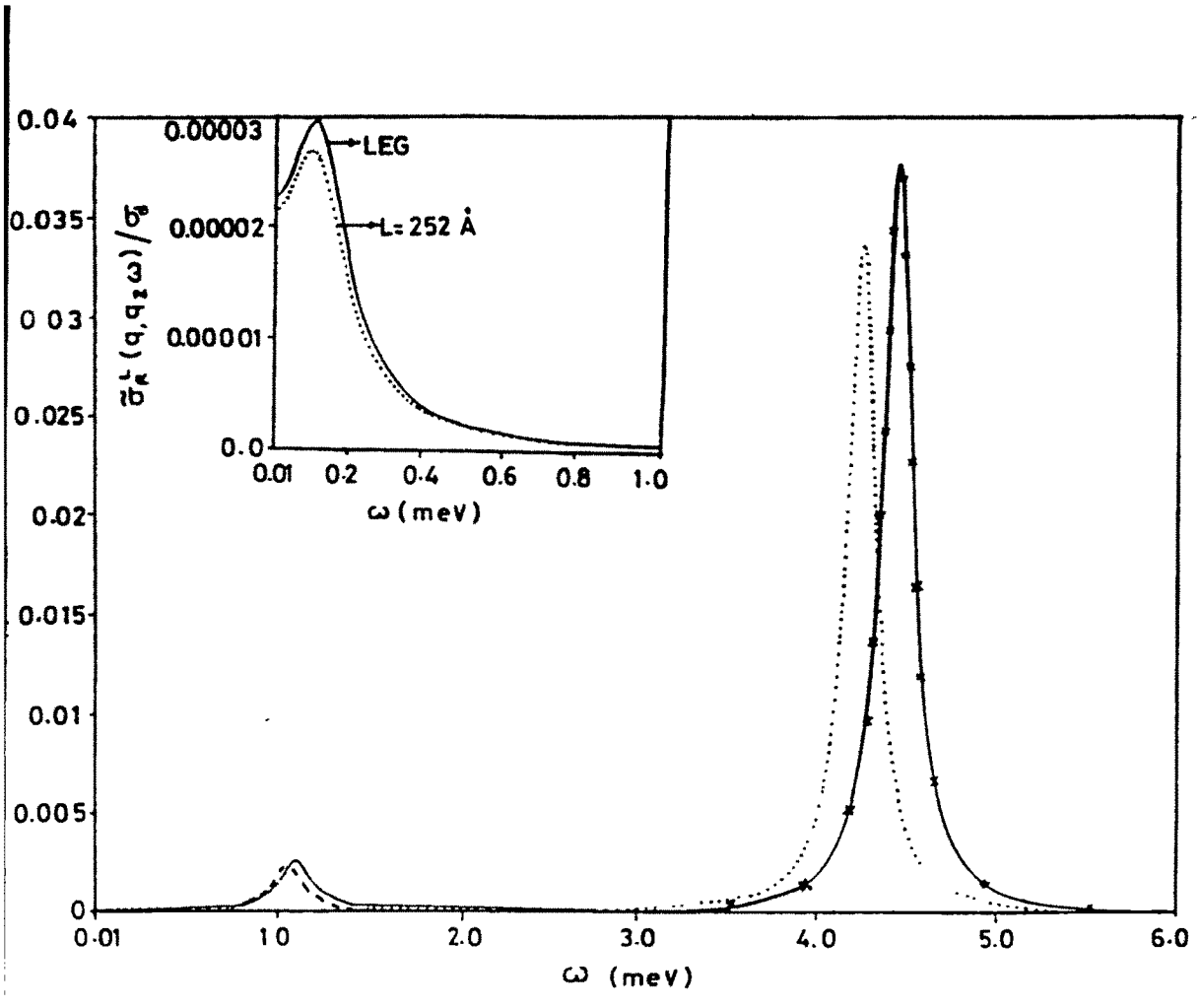

Fig. 3.4 The $\tilde{\sigma}^{L}_{R}(\mathbf{q},q_z,\omega)/\sigma_d$ is plotted as a function of ω for qd=0.01 (inset curve) qd=0.1(dashed curve for L=252 Å and solid line curve for LEG) and qd=0.4 (dot-dot curve for L=252 Å and solid line curve with crosses for LEG) at $\cos(q_z d)$= -1, n_s=7 3 x10^{11} cm^{-2} and γ=0.1meV.

$$F(\mathbf{q},q_z,\omega) = 1+(d/a^*)\,(\eta v_F/c)^2 U(\mathbf{p},q_z)\,U(\mathbf{q},q_z)\,(\mathbf{q}/\mathbf{p})\,\{1+1/3\eta)$$
$$[(\eta^2-1)/\eta\bar{\mathbf{q}}-1)(\eta^2-1-\eta\bar{\mathbf{q}})^{1/2}-((\eta^2-1)/\eta\bar{\mathbf{q}}+1)(\eta^2-1+\eta\bar{\mathbf{q}})^{1/2}]\}$$
$$-(\eta v_F/c)^2\,(\mathbf{qd}/2)(\mathbf{q}/\mathbf{p})\,U(\mathbf{p},q_z)[\varepsilon_0-1]. \qquad (3.29)$$

The $\varepsilon^L(\mathbf{q},q_Z,\omega)$ goes to zero at $\eta=\mathbf{q}v_F\omega_L$, where ω_L is

$$\omega_L(q,q_z) = qv_F/\{1-[1/(1+qa^*/2U(q,q_z))]^2\}^{1/2}, \qquad (3.30)$$

where $a^*=\hbar^2\varepsilon_0/m^*e^2$ and ω_L is the plasma frequency for SL, which attains maximum value at $q_Zd=0$ and it reduces to $(4\pi n_S e^2/m^*\varepsilon_0)^{1/2}$ when both q_Zd and $\mathbf{q}d$ are zero. ω_L goes to zero for $\mathbf{q}d\to 0$ at $q_Zd\neq 0$. $\tilde{\sigma}_R^L(\mathbf{q},q_Z,\omega)$ as function of ω shows a peak around $\omega=\omega_L$ for given values of $\mathbf{q}$ and q_Z. $\tilde{\sigma}_R^L(\mathbf{q},q_Z,\omega)$ is real part of $\sigma^L(\mathbf{q},q_Z,\omega)$. The peak which corresponds to single particle excitations is smeared out in $\tilde{\sigma}_R^L(\mathbf{q}.q_Z,\omega)$ because of the screening which prominently affects the $\tilde{\sigma}_R^L(\mathbf{q},q_Z,\omega)$ at all values of $\mathbf{q}$ and q_Z for $\omega<\omega_L$. Computed $\tilde{\sigma}_R^L(\mathbf{q},q_Z,\omega)$ is plotted in Fig.3.4 as a function of ω for three values of $\mathbf{q}d$ (0.01, 0.1 and 0.4) at $\cos(q_Zd)= -1$, $n_S=7.3\times 10^{11}$ cm^{-2} and $\gamma=0.1$ meV for two cases of L=252 Å as well as for L<<d (LEG case). Away from peak, $\tilde{\sigma}_R^L(\mathbf{q},q_Z,\omega)<<\tilde{\sigma}_R^L(\mathbf{q}.q_Z,\omega)$, which underlines importance of screening effects. The peak height enhances, peak width decreases and peak position shifts toward higher values of ω on increasing $\mathbf{q}$ at all values of $\cos(q_Zd)$ We have also found that $\mathbf{q}$-dependence of position, height and width of the peak is maximum for $\cos(q_Zd)=-1$ and weakest for $\cos(q_Zd)=1$. It is to be mentioned that the half width of a peak in $\tilde{\sigma}_R^L(\mathbf{q}.q_Z.\omega)$ is the measure of damping of plasma oscillations. The increase in L from L<<d (LEG case) to 252 Å reduces the peak height and shifts the peak positions toward lower values of ω, whereas half width of peak remains almost unchanged at all $\mathbf{q}$-values, as can be seen from the figure. $\tilde{\sigma}_R^L(\mathbf{q},q_Z,\omega)$ has also been computed as a function of ω for different values of q_Zd. It is found that peak height reduces and peak position shift towards lower ω-values on changing $\cos(q_Zd)$ from 1 to -1

The $\tilde{\sigma}^T(\mathbf{q},q_Z,\omega)$ has poles on both real as well as imaginary axis of ω. The $\tilde{\sigma}_R^T(\mathbf{q},q_Z,\omega)$ and $\tilde{\sigma}_I^T(\mathbf{q},q_Z,\omega)$, real and imaginary parts of $\sigma^T(\mathbf{q},q_Z,\omega)$, respectively are plotted for $\mathbf{q}d=0.1$, $q_Zd=0.1$ and $\gamma=0.1$ meV (i) in Fig.3.5a as a function of $i\omega$ on replacing $(\omega+i\gamma)$ by $(i\omega-\gamma)$ in (3.12), and (ii) in Fig.3.5b as a function of ω when $\eta=(\omega+i\gamma)/\mathbf{q}v_F$ It is interesting to note that behaviors of $\tilde{\sigma}_R^T(\mathbf{q},q_Z,\omega)$ and $\tilde{\sigma}_I^T(\mathbf{q},q_Z,\omega)$ versus $i\omega$ for $\omega\leq\omega_P$ are similar to those of $\tilde{\sigma}_I^T(\mathbf{q},q_Z,\omega)$ and $\tilde{\sigma}_R^T(\mathbf{q},q_Z,\omega)$ versus ω for $\omega>\omega_L$, respectively. Also, $\tilde{\sigma}^T(\mathbf{q},q_Z,\omega)$ near pole on

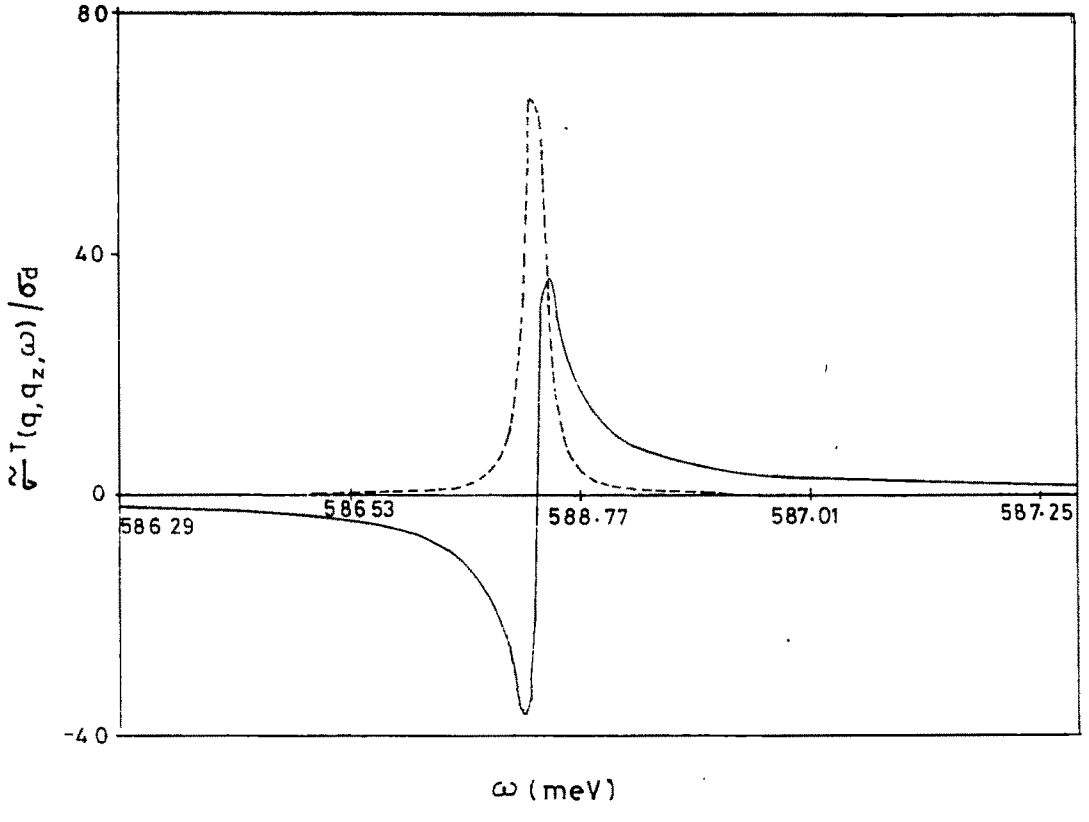

Fig. 3.5a The $\sigma_R^T(\mathbf{q},q_z,\omega)/\sigma_d$ (solid line) and $\sigma_I^T(\mathbf{q},q_z,\omega)/\sigma_d$ (dotted curve) for $\mathbf{q}d=0.1$, $q_zd=0.1$ and $\gamma=0$ 1 meV are plotted as a function of ω.

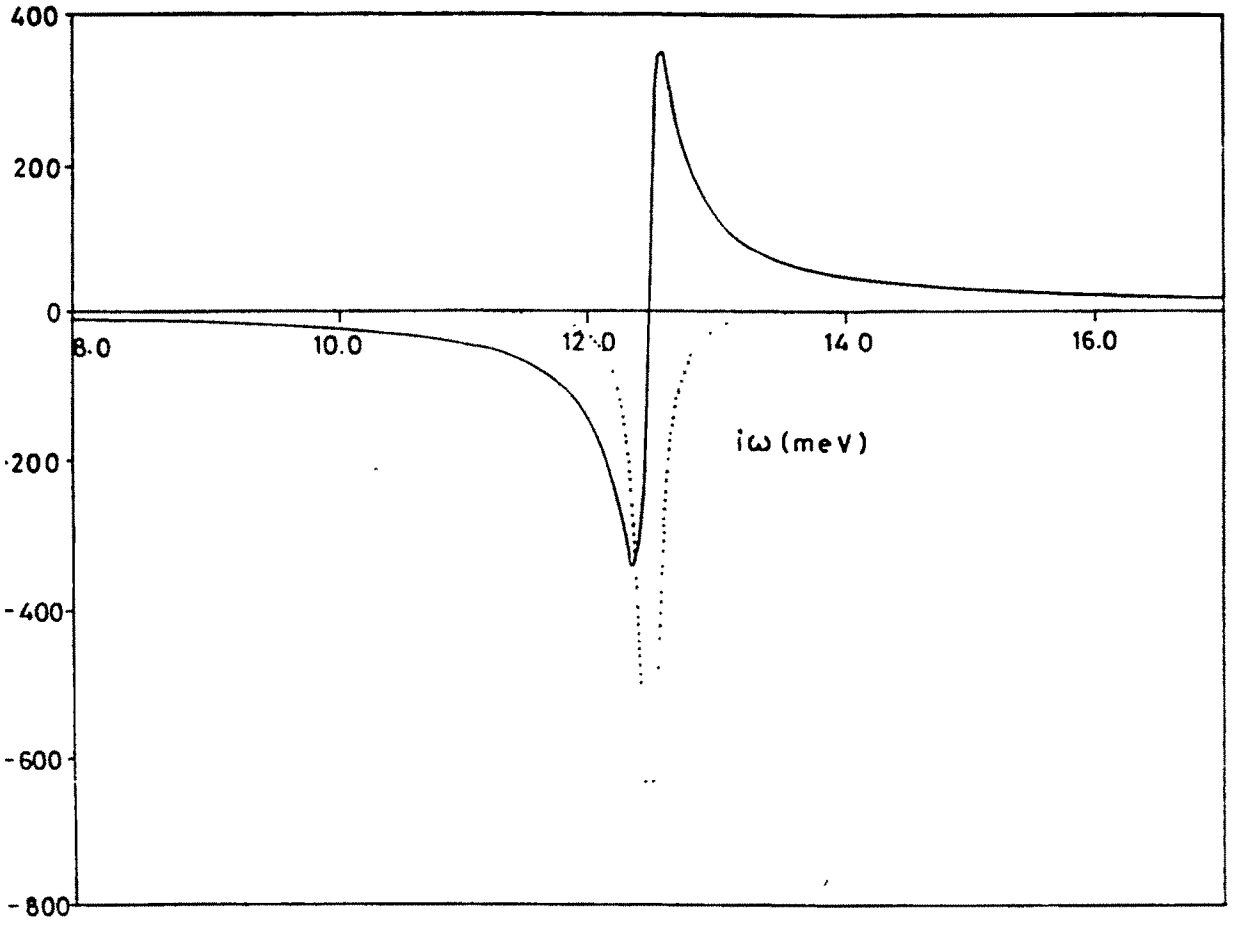

Fig 3.5b The $\tilde{\sigma}_R^T(\mathbf{q},q_z,\omega)/\sigma_d$ (solid line) and $\tilde{\sigma}_I^T(\mathbf{q},q_z,\omega)/\sigma_d$ (dotted curve) for $\mathbf{q}d=0.1$, $q_zd=0.1$ and $\gamma=0.1$ meV are plotted as a function of $i\omega$.

iω-axis is negative and its magnitude is quite large, whereas $\tilde{\sigma}^T(\mathbf{q},q_z,\omega)$ near pole on ω-axis is very small and positive. From Fig.3.5a it can be concluded that there exists a collective state at imaginary ω-axis for real values of **q** and q_z. The poles on imaginary ω-axis for both **q** and q_z real correspond to damped polaritons and they exist for $|\omega| \leq \omega_L$. We found that the poles in $\tilde{\sigma}^T(\mathbf{q},q_z,\omega)$ on imaginary axis disappear when we use $\alpha_e^T(\mathbf{q},\omega) \sim -nq^2/m^*\omega(\omega+i\gamma)$ and take 2D definition of current density. For better understanding of our results and the origin of poles in $\tilde{\sigma}^T(\mathbf{q},q_z,\omega)$ on imaginary value ω-axis, we consider the case of $\mathbf{q}v_F << \omega \sim \mathbf{q}c$ and simplify $\alpha_e^T(\mathbf{q},\omega)$ and $U(\mathbf{q},q_z)$. The $F(\mathbf{q},q_z,\omega)=0$ which describes the condition of propagation of transverse electromagnetic modes (TEM), for $\mathbf{q}v_F << \omega \sim \mathbf{q}c$ reduces to

$$\eta^4(\alpha^2-2\alpha\beta)+\eta^2(\beta^2-2\alpha+2\beta)+1=0, \tag{3.31}$$

where

$$\alpha(\mathbf{q},q_z) = (v_F/c)^2\,(\mathbf{q}d/2)\,[U'(\mathbf{q},q_z)+\varepsilon_0] \tag{3.32a}$$

and

$$\beta(\mathbf{q},q_z) = (v_t/c)^2\,(d/a')\,U(\mathbf{q},q_z)\,U'(\mathbf{q},q_z) \tag{3.32b}$$

with

$$U'(\mathbf{q},q_z)= qd\,/\,[1+(qd)^2/2-\cos(q_zd)]. \tag{3.33}$$

Solution of Eq.(3.31) gives

$$\omega_{\pm}(\mathbf{q},q_z)=[-(\beta^2+2\beta-2\alpha)\pm\beta(\beta^2+4\beta-4\alpha+4)^{1/2}]\,(\mathbf{q}v_F)\,/(2\alpha^2-4\alpha\beta)^{1/2} \tag{3.34}$$

The $\beta/\alpha=2U/qa^*$ which is found to be larger than unity for all possible values of **q** and q_z. In following we consider four possible cases

(i) $U(\mathbf{q},q_z)$ and $U'(\mathbf{q},q_z)$ are positive and real when both **q** and q_z are real or **q** is real and q_z is imaginary but $|q_z| < q$. Both α and β are positive to give rise real ω_- and imaginary ω_+. Also, $\omega_+ < \omega_L$ and $\omega_- > \omega_L$ at all values of **q** and q_z. When both **q** and q_z are real, TEM wave has dispersive behavior in x-y plane as well as along z-axis of CSSL1. When q_z is imaginary and **q** is real, TEM wave is attenuated along z-axis and dispersed in x-y plane.

(ii) $U(\mathbf{q},q_z)$ and $U'(\mathbf{q},q_z)$ are negative and real when q_z is imaginary and $\mathbf{q}$ is real and they obey $|q_z| > \mathbf{q}$. The TEM wave is attenuated along z-axis and it disperses in x-y plane. α is negative and β is positive. Both ω_+ and ω_- lie on imaginary axis of frequency.

(iii) $U(\mathbf{q},q_z)$ and $U'(\mathbf{q},q_z)$ are imaginary and positive when $\mathbf{q}$ is imaginary and q_z is real and they satisfy $q_z > |\mathbf{q}|$. Both α and β are negative. The ω_- lies on imaginary axis whereas ω_+ lies on real axis of ω. In this case, TEM wave is attenuated in x-y plane and it disperses along z-axis.

(iv) $U(\mathbf{q},q_z)$ and $U'(\mathbf{q},q_z)$ are imaginary and negative for when $\mathbf{q}$ is imaginary and q_z is real and they satisfy $(1-\cos(q_z d)) < (1-\cosh(qd)) < |(\mathbf{q}d)^2|/2$. The TEM wave is attenuated in x-y plane and it disperses along z-axis. α is positive and β is negative. We find that both ω_+ and ω_- lie on real axis of ω for $|\beta| > 2$ and they lie on imaginary axis of ω for $|\beta| < 2$.

Above analysis of our results suggests that F=0 yields real as well as imaginary roots of ω The positive real value of $\omega_{\pm}(\mathbf{q},q_z)$ corresponds to frequency of a well-defined transverse collective excitation mode whereas imaginary root presents a collective excitation mode

The inverse of $\mathbf{q}$ when it is imaginary describes penetration depth in x-y plane. Equation (3.29), along with (3.25), shows that F=0 could only be satisfied when $|\mathbf{q}|$ and $|q_z|$ are of same order In case of $|\mathbf{q}d|$ and $|q_z d|$ not much smaller than unity, penetration depth is found to be almost independent of ω. Equation (3 34) can further be simplified for $\mathbf{q}d \ll 1$ and $q_z d \ll 1$ to obtain

$$\omega_-^2 = \omega_p^2 / [1+(q_z/\mathbf{q})^2] + c^2(\mathbf{q}^2+q_z^2), \qquad (3.35a)$$

and

$$\omega_+^2 = -\mathbf{q}^2(\mathbf{q}^2+q_z^2)^2 (a' d^2/2)^2 \omega_-^2. \qquad (3.35b)$$

As mentioned above, in case (iv). both ω_+ and ω_- are real for $|\beta| > 2$. Solution of Eq. (3.35a) for $\lambda_1 (=1/i\mathbf{q})$ when $q_z \ll |\mathbf{q}|$ gives $\lambda_1 = c/\sqrt{\omega_p^2 - \omega^2}$, which is usual penetration depth defined in text books However, on computing Eq.(3 35b) for $\lambda_2 (=1/i\mathbf{q})$ when $q_z \ll |\mathbf{q}|$, we find that λ_2 decreases with ω and Eq (3.35b) can only be satisfied for of $\omega_+ \leq 3\times10^4$ Hz at all values of q_z. Our computed λ_2 is plotted as a function of ω in Fig.3 6 at different values of $q_z d$. We find that λ_2 is almost proportional to $\omega^{-1/3}$

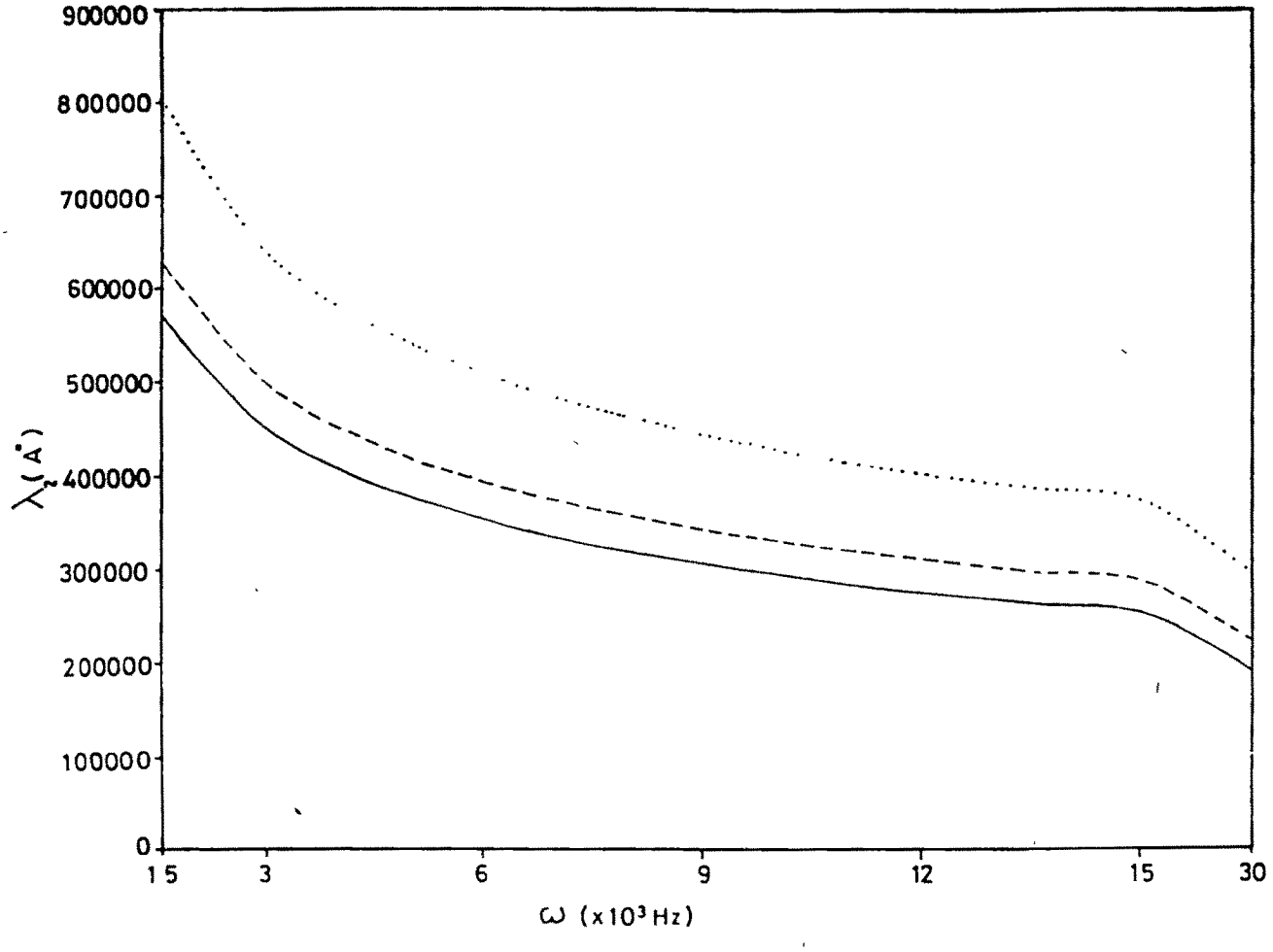

Fig. 3.6 The computed λ_2 is plotted as a function of ω for q_z=0.0 (solid line curve), q_z=0.5 $|\mathbf{q}|$ (dashed curve) and q_z =0.8 $|\mathbf{q}|$ (dotted curve).

3.5 Conclusion

Longitudinal and transverse conductivities are computed for modulation doped $GaAs/Ga_XAl_{1-X}As$ superlattice by taking into account screening effects and the finite width of an electron layer. Our calculated macroscopic conductivity significantly differs from Drude conductivity, even in long wavelength limit ($qd<<1$ and $q_Zd<<1$), for $qv_F\sim(\omega+i\gamma)$. $\sigma_R^L(q,q_Z,\omega)$ versus ω exhibits a peak which corresponds to single particle excitations, whereas $\sigma_R^T(q,q_Z,\omega)$ versus ω does not shows any peak. $\sigma_R^{L/T}(q,q_Z)$ as a function of q_Zd shows oscillatory behaviour which is characteristic of periodic structure of a SL. The amplitude of oscillations decreases on increasing qd. In case of $\tilde{\sigma}_R^L(q,q_Z,\omega)$, peak height reduces and peak position shifts toward the lower values of ω, whereas half width of peak remains almost unchanged on replacing LEG model by a more realistic model which takes into account finite width of an electron layer for given values of q and q_Z. $\omega_+(q,q_Z)$ and $\omega_-(q,q_Z)$ can be real as well as imaginary, depending on q and q_Z. The real value of $\omega_+(q,q_Z)$ lies below microwave frequency range. Imaginary value of $\omega_\pm(q,q_Z)$ belongs to a collective state whose presence can be seen in $\tilde{\sigma}^T(q,q_Z,\omega)$ and it is called as ghost polariton state There are two penetration depths, λ_1 and λ_2 which correspond to ω_- and ω_+, respectively λ_1 increases, whereas λ_2 decreases with ω. λ_2 belong to frequencies below microwave frequency regime.

REFERENCES

[1] J.J. Quinn, G Eliasson and P. Hawrylak, "Spatial Dispersion in Solids and Plasmons" (edited by P. Halevi), Chapter 4, P.243, Elsevier Science Publishers B.V. (1992) and references therein.

[2] A.C. Sharma , R. Sen and P. Tripathi, J. Phys.: Condens. Matter 9, 8041 (1997).

[3] A.C. Tselis and J.J. Quinn, Phys. Rev. B 29, 3318 (1984).

[4] J.K. Jain and P.B. Allen, Phys. Rev. B 32, 997 (1985).

[5] R.E. Camley and D.L. Mills, Phys. Rev. B 29, 1695 (1984).

[6] A.L. Fetter, Ann. Phys. (N.Y) 88, 1 (1974).

[7] X. Zhu, X Xia, J.J. Quinn and P. Hawrylak, Phys Rev. B 38, 5617 (1988).

[8] N.C. Constantinou and M.G. Cottam, J. Phys C: Solid State Phys. 19, 739 (1986).

[9] O. Olego, A Pinczuk, A.C Gossard and W Weigmann, Phys. Rev B 25, 7867 (1982).

[10] G. Scamario, M. Haines, G. Abstreiter, E Molinari, S. Baroni, A Fisher and K. Ploog, Phys. Rev. B 47, 1483 (1993)

[11] L. Zheng and S Das Sarma, Phys. Rev. B 53, 9964 (1996)

[12] A.C. Sharma and A K. Sood, J. Phys.: Condens. Matter 6, 1553 (1994)

[13] S.P. Apell and O. Hunderi, "Hand Book of Optical Constant of Solids II" (Academic Press, 1991) and references therein.

[14] C.W.J Beenakker and H. Van Houten, in Solid State Phys. Vol. 44 (ed) H Ehrenreich and D Turnbull, (Academic, New York, 1991).

[15] R.D. King-Smith and J.C Inkson, Phys. Rev B 36, 4796 (1988).

[16] H. Shi and A. Griffin, Phys. Rev. B 44, 11977 (1991).

[17] K.I. Golden and G. Kalman, Phys. Rev. B 45. 5834 (1991); Phys. Rev. B 52, 14719 (1995); Phys. Rev. B 57, 9883 (1998).

[19] R.Q. Yang, X.J. Lu and C. Tsai, J. Phys. C: Solid State Phys. 21, L91 (1988).

[20] A. Sibille, J.F. Palmier, H. Wang and F. Mollot. Phys. Rev. Lett. 64, 52 (1989).

[21] X.L. Lei and I.C. da Cunha Lima, J. Appl. Phys. 71, 5517 (1992).

[22] Grahn. K. von Klitzing, K. Ploog and G.H. Dohler. Phys. Rev. B 43, 12094 (1991).

[23] X.J. Lu and N.J.M. Horing, Phys. Rev. B 44. 5651 (1991).

[24] R.Q. Yang, J. Phys.: Condens. Matter 1, 7925 (1989).

[25] K. Takayanagi and E. Lipparini. Phys. Rev. B 56. 872 (1997).

[26] J.P. Eisenstein. L.N. Pfeiffer and K.W. West, Phys. Rev. B 68. 674 (1992).

[27] D. Pines and P. Nozieres, "The Theory of Quantum Liquids" (Benjamin, New York. 1966), Vol. I.

[28] F. Stern. Phys. Rev. Lett. 18. 546 (1967).

[29] H. Morkoe in "The Technology and Physics of Molecular Beam Epitaxy", (ed.) E.H.C Parker. Chap. 7. (Plenum Press. New York. 1985).

[30] T. Saku, Y Horikoshi and Y. Tokura. Jpn. J. Appl. Phys. 35, 34 (1996).

[31] K. Ploog. J. Vac. Sci. Techol. 16, 838 (1979)